All-optical thermal microscopy of laser excited waveguides

Ruiyun He,[1,2] Javier Rodríguez Vázquez de Aldana,[3] Ginés Lifante Pedrola,[2] Feng Chen,[1] and Daniel Jaque[2,*]

[1]*School of Physics, State Key Laboratory of Crystal Materials and Key Laboratory of Particle Physics and Particle Irradiation (MOE), Shandong University, Jinan 250100, China*
[2]*Fluorescence Imaging Group, Departamento de Física de Materiales, Facultad de Ciencias, Universidad Autónoma de Madrid, 28049 Madrid.*
[3]*Aplicaciones del Láser y Fotónica (ALF-USAL), Universidad de Salamanca, Salamanca 37008, Spain.*
**Corresponding author: daniel.jaque@uam.es*

Received XX Month XXXX; revised XX Month, XXXX; accepted XX Month XXXX; posted XX Month XXXX (Doc. ID XXXXX); published XX Month XXXX

We report on an unique combination of high-resolution confocal microscopy and ratiometric luminescence thermometry to obtain thermal images of 800 nm pumped ultrafast laser inscribed waveguides in a Nd:YAG crystal. Thermal images evidence a strong localization of thermal load in the waveguide active volume. Comparison between experimental data and numerical simulations reveals that ultrafast laser inscribed damage tracks in Nd:YAG crystals behave both as low-index and low-thermal conductivity barriers. © 2016 Optical Society of America

OCIS codes: *(110.6820) Thermal imaging; (230.7380) Waveguides, channeled; (160.5690) Rare-earth-doped materials; (300.6280) Spectroscopy, fluorescence and luminescence; (140.3390) Laser materials processing.*

http://dx.doi.org/10.1364/OL.99.099999

The appearance of light-induced temperature increments and temperature gradients is known to be one of the most critical parameters affecting photonic devices. As a widely studied example, pump-induced temperature increments in high power lasers have been demonstrated to be a limiting factor [1,2]. As a matter of fact, efficient heat dissipation in high-power solid-state lasers has been the object of extensive studies as a result of the appearance of sophisticated and efficient temperature stabilization systems. Temperature effects are expected to be even more critical and relevant in integrated photonic devices based on optical waveguides. Note that the performance of such elements is based on a reduced (10^{-2}-10^{-3}) refractive index contrast. Since refractive index is, in most of the cases, a temperature dependent magnitude, the existence of local thermal loadings can lead to a modification of the refractive index contrast and, therefore, the confinement properties of the waveguide [3]. In addition, thermal measurements in optical waveguides are also of great interest from a pure fundamental point of view. Fabrication of optical waveguides requires micro-structural modification of an initially homogeneous material. Intra-waveguide thermal imaging is essential to study how heat dissipation and diffusion takes place in such micro-structured materials. Despite its great interest from an applied and fundamental point of view, thermal imaging of optical waveguides still remains as an almost unexplored research field.

The lack of experimental data concerning thermal imaging of optical waveguides resides on the fact that the typical methods used for thermal imaging (such as infrared thermography) cannot be applied due to the micrometric dimensions of the optical active volume [4,5]. Experimental techniques for thermal imaging of waveguides should satisfy several requirements: sub-micrometric spatial resolution, sub-degree thermal sensitivity and complete absence of any physical contact. These three technical requirements are simultaneously satisfied by Confocal Luminescence Thermometry (CLT), which is based on the extraction of thermal information from an appropriate analysis of the confocal fluorescence images of micro-sized devices. CLT has already been demonstrated to be a flexible and sensitive technique capable of providing three dimensional thermal images of luminescent systems [6-8]. Nevertheless its potential application for the acquisition of thermal images of integrated waveguides has not been yet demonstrated.

In this letter we provide experimental evidence of how high-resolution CLT can be successfully applied to obtain thermal images of active waveguides in presence of optical excitation. In particular, this possibility has been demonstrated in Ultrafast Laser Inscribed (ULI) waveguides fabricated in Nd:YAG laser crystals and ceramics that are becoming one of the most promising, cost-effective and flexible integrated devices [9-12]. The role played by the laser-modified local thermal conductivity of the Nd:YAG network on the spatial distribution of pump-induced heating is also discussed by comparing thermal and micro-structural images obtained by conventional confocal fluorescence microscopy.

A schematic of the experimental setup used all along this work is included in Fig. 1(a). The surface channel waveguide is fabricated by using an amplified Ti:sapphire laser system (Spitfire, Spectra Physics), generating linearly polarized 120 fs pulses at 800 nm, with 1 kHz repetition rate and 1 mJ maximum pulse energy at the Universidad de Salamanca, Spain. The fs laser beam was focused by a microscope

objective (Leica 40×, 0.65 N.A.). A Nd:YAG crystal (1% Nd^{3+} doping) was placed on a motorized 3-axes stage and scanned at a constant speed (500 μm/s), producing parallel damage tracks with pre-tailored depths and separations. Top inset in Fig. 1(a) shows an optical transmission image of the waveguide cross section in which the presence of the damage tracks is clearly observed. Seven damage tracks were inscribed forming a pseudo semi-circle close to the crystal surface so that light could be confined between crystal-air interface and the low-refractive index circular barrier [12].

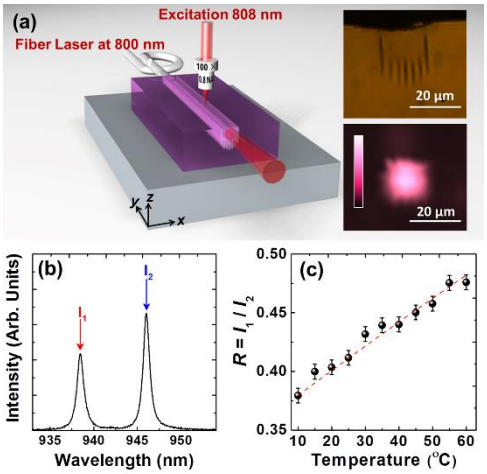

Fig. 1. (a) Schematic of the experimental setup. Insets show (top) the microscope image of the waveguide endface and (bottom) the spatial modal distribution at 800 nm. (b) Normalized micro-luminescence emission spectra around 940 nm. The two emission lines used for ratiometric thermal sensing are indicated. (c) Intensity ratio R as a function of temperature. Dots are experimental data and dash line corresponds to the linear fit.

Thermal loading in the Nd:YAG waveguide was investigated by using a "pump and probe" setup. The "pump" radiation was provided by an 800-nm laser diode coupled to a single-mode fiber that is pigtailed into one of the ends of the waveguide (Fig. 1(a)). The bottom inset in Fig. 1(a) shows the waveguide mode at 800 nm as measured at the exit face of the waveguide, showing clear confinement between damage tracks and crystal surface. The Nd:YAG waveguide is placed into a home-made high resolution confocal microscope equipped with a 3-axes motorized stage. A second 808-nm laser beam (low power), serving as a "probe" beam, is focused into the sample by using a single long-working-distance microscope objective (100×, 0.80 NA). The 808-nm laser radiation is absorbed by the Nd^{3+} ions ($^4I_{9/2} \rightarrow {}^4F_{5/2}$ transition) and the subsequent luminescence generated in the 920-950 nm spectral range, corresponding to the high energy lines within the $^4F_{3/2} \rightarrow {}^4I_{9/2}$ transition [13], is collected by the same microscope objective. This luminescence is spectrally and spatially cleaned by different filters and apertures and, finally, spectrally analyzed by a high resolution spectrometer. A typical microluminescence spectrum obtained in our experimental conditions is shown in Fig. 1(b). We focus on the spatial variation of the spectral properties of these two particular emission lines as they have demonstrated to be excellent probes to detect slight modifications in the microstructural properties of the YAG network [14]. In addition, recent works have demonstrated that the ratio between the emission intensities of these two lines was also used for high resolution remote temperature sensing [15]. Figure 1(c) shows the intensity ratio $R = I_1/I_2$, where I_1 and I_2 are the luminescence emitted intensities at 938 and 946 nm as obtained for different temperatures of the Nd:YAG crystal. From this calibration curve, obtained by placing the Nd:YAG crystal on a temperature controlled microscope stage, a pseudo-linear relation (arising from temperature induced population re-distribution among $^4F_{3/2}$ sub-stark levels) is clearly observed. Such linear relation allows for a ratiometric simulation of temperature with a sensitivity close to 0.5% $°C^{-1}$. Thus, simultaneous cross-sectional scanning of the 808 nm "probe" spot and spectral analysis of collected luminescence provides simultaneously micro structural (damage, stress and disorder) and thermal images of the waveguide. It is important to note that the power of the "probe" beam is not larger than 20 mW so that it induced a negligible local heating.

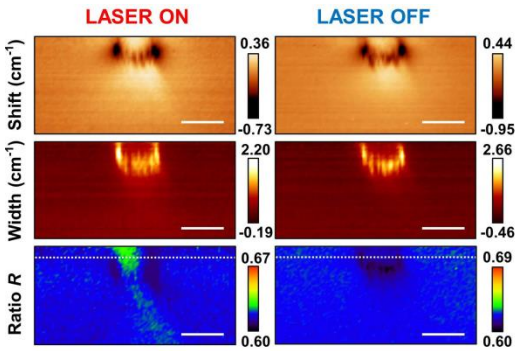

Fig. 2. Cross-sectional confocal fluorescence images of the ULI waveguide in Nd:YAG as obtained in terms of the spatial variation of the spectral shift, linewidth of the 945 nm emission line and the intensity ratio R, obtained with (right column) and without (left column) of 800 nm radiation propagating along the waveguide. Scale bar is 20 μm in all the cases.

Figure 2 presents the confocal fluorescence images of the waveguide´s cross section based on the spatial variation of the spectral shift and width of the emission line at 945 nm, with and without 800-nm "pump" laser radiation propagating along the waveguide. These images were obtained at a distance of 100 μm from the waveguide´s input face. From these fluorescence images it is clear that damage tracks are characterized by a broadening of the emission lines. This suggests the presence of well localized damage of the Nd:YAG network [14]. This local damage is accompanied by a redshift that is attributed to a local densification at the damage tracks that is mechanically compensated by a local dilatation at their apexes [15]. Based on previous works we conclude that ULI waveguides in crystalline materials are typically characterized by a low index (damage) cladding and a high index (compressed) core leading to strong light confinement between the crystal-air interface and the damage tracks (as observed in the inset of Fig. 1(a)).

The bottom row in Fig. 2 includes the fluorescence cross-sectional images of the waveguide as obtained in terms of the spatial variation of the intensity ratio R that is unequivocally related with the local Nd:YAG temperature. In this case, the cross-sectional fluorescence image of the waveguide was strongly modified with the 800 nm "pump" laser radiation propagating along the waveguide. Such change is further evidenced in Fig. 3 (a) that shows the intensity ratio profiles obtained by the excitation beam scanning parallel to crystal surface (x axis in Fig. 1(a)) at a depth of 5 microns either in presence or absence of 800 nm propagating radiation (the scan lines are indicated in Fig. 2 by dashed lines). In absence of "pump" radiation propagating along the waveguide, the intensity ratio is far from being constant. Indeed, the ratio decreases at the damage tracks and at the waveguide volume. The exact reason for this decrease in absence of pump radiation propagating along the waveguide is not fully understood but is very likely related to a different damage-induced quenching of the two fluorescence lines used for the evaluation of the intensity ratio. Regardless of the exact origin of this ratio decrease at tracks and at waveguide volume, what it is clear from

Fig. 3(a) is that when "pump" radiation is propagating along the waveguide, the intensity ratio profile is clearly modified. A slight increment in the ratio is found in the waveguide´s surroundings whereas inside the waveguide the ratio increment becomes more pronounced. These changes are attributed to the temperature increment caused by the "pump" 800 nm radiation.

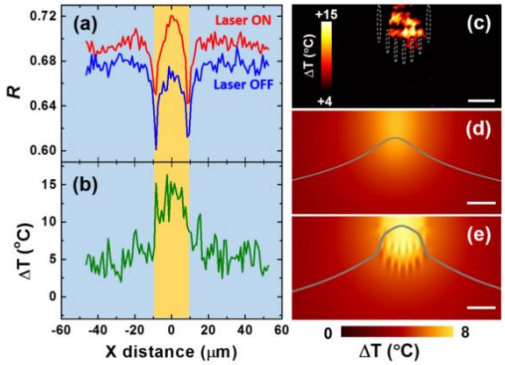

Fig. 3. (a) Variation of the intensity ratio *R* as obtained along the horizontal scans schematically indicated in Fig. 2 in presence and absence of 800 nm laser radiation. (b) Temperature increment profile calculated from (a). (c) Cross sectional thermal image of the Nd:YAG waveguide. Dashed lines indicate the position of damage tracks. All experimental data were obtained for 100 mW of injected power at a distance of 100 μm from the input face. Calculated thermal image of waveguide assuming (d) a homogeneous thermal conductivity or (e) a localized thermal conductivity reduction at damage tracks. Gray lines are obtained at a depth of 5 μm. Scale bar is 10 μm in (c)-(e).

The temperature profile can be now calculated by taking the "laser-off" profile as background and by using the calibration curve of Fig. 1(c). Results are shown in Fig. 3(b), from which several conclusions can be extracted. The first one is that, in our experimental conditions, the laser induced thermal load in ULI Nd:YAG waveguides is in the order of a few degrees. Secondly, although the partial absorption of the 800 nm laser radiation causes a slight temperature increment in the waveguide surroundings, the temperature increment is well localized at the waveguide´s volume. This is further ratified by the thermal image included in Fig. 3(c), obtained by analyzing the ratio-based fluorescence images of Fig. 2. The strong spatial localization of the laser-induced heating suggests that the damage tracks are behaving as a material volume with large thermal impedance capable of producing strong thermal confinement. This is, indeed, in agreement with the results published by Y. Bellouard *et al.* [17] who concluded that ultrafast laser induced damage tracks produced in transparent materials are characterized by a reduced thermal conductivity that was tentatively explained to be caused by a local increment in the probability of phonons scattering events due to a large density of defects. Figures 2 and 3 reveal that the moderate temperature change induced in the waveguide by the "pump" beam affect neither the stress field nor the damage pattern (shift and width images in Fig. 2 are not affected by the presence of the "pump" beam). Note that this conclusion is valid for the laser powers and maximum temperature increments found in this work, but it is not general. For larger pump powers and temperature increments the induced modifications in stress fields or the possible presence of self-annealing processes could not be neglected. Finally, from data included in Fig. 3(b) we have estimated thermal gradients at the edge of the waveguide close to 0.5 °C/μm that are more than one order of magnitude larger than the thermal gradients observed in laser crystals [18].

The effect that the reduction of thermal conductivity at damage tracks has on the spatial distribution of the laser induced temperature increment has been also investigated by performing numerical simulations of the thermal diffusion equation using a finite difference approach. Thermal and spectroscopic properties assumed in our calculations were the same as that used by M. E. Innocenzi *et al.* [19]. Fig. 3(d) shows the calculated steady state temperature distribution caused by the 800-nm radiation propagating along the waveguide, assuming a homogeneous thermal conductivity (i.e. assuming that the ULI process does not modify the original thermal conductivity of the YAG network). In absence of any modification of thermal conductivity the temperature increment spreads out of the waveguide volume due to heat diffusion. Fig. 3(e) shows the steady state temperature distribution when a severe (80 %) decrease in the thermal conductivity at damage tracks is assumed. Such reduction of 80% in the thermal conductivity at damage tracks was found to provide the best agreement between calculations and experimental data. Note that this assumed value is found reasonable when it is compared with the damage level caused by ULI in the Nd:YAG network that has been previously reported to range between 50 and 70% [14,20]. In this case, although temperature increments are also produced in the surroundings of the waveguide, laser-induced temperature increment is mainly localized at the waveguide volume. This is further evidenced in the horizontal temperature profiles included as gray lines in Figs. 3(d) and 3(e) that has been obtained at a depth of 5 μm. Although not being identical, the calculated thermal profile well reproduces the main features of the experimental data included in Fig. 3(b): There is a slight temperature increment in the surroundings of the waveguide but thermal loading is mainly taking place in the waveguide volume. At this point it should be noted that although the numerical calculations reproduced qualitatively the experimental temperature patterns, a quantitative discrepancy is observed. While numerical simulations predict a temperature increment of 8 °C within the waveguide volume, experimental measurements reveal a larger temperature increment of 15 °C. The origin of this discrepancy is not fully understood at this moment but we state that it could be due to different reasons including the variation of the fractional thermal loading of Neodymium ions inside the waveguide´s volume or to the presence of heating centers associated to the formation of lattice defects. Nevertheless, what is clear from both the experiments and simulations presented here is that the magnitude of the laser induced thermal loading is of a few degrees.

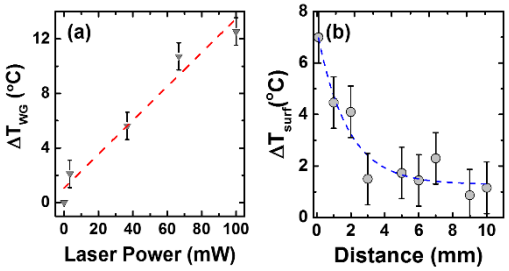

Fig. 4. (a) Waveguide temperature increment as a function of the 800 nm "pump" laser power at a fixed distance of 100 μm from input face. (b) Temperature increment for a fixed 800 nm injected laser power of 100 mW as a function of the distance from the input face. Dots are experimental data and dashed lines are the best fits to (a) linear and (b) exponential function.

The maximum temperature increment induced inside the waveguide (ΔT_{WG}) was also measured as a function of the "pump" laser power injected into the waveguide at a fixed location (100 μm from the waveguide´s input face) as shown in Fig. 4 (a). Figure 4 (b) depicts the surface temperature increment (ΔT_{surf}) at different distances from the

input face for a fixed injected laser power (100 mW). Note that laser induced heating was found to increase linearly with the injected 800 nm laser power and to decrease exponentially with the propagation length along the waveguide as it was, indeed, expected.

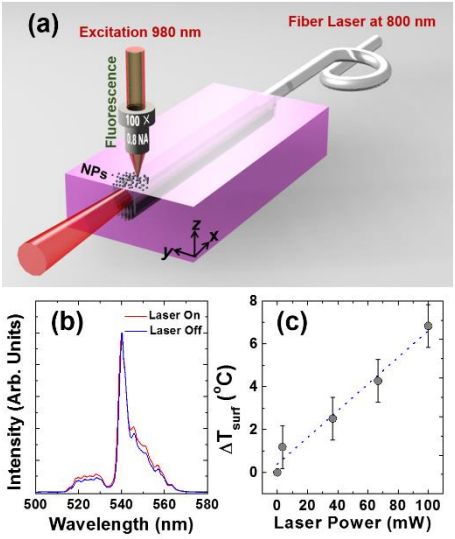

Fig. 5. (a) Schematic of the experimental setup used for surface temperature determination using Er:Yb:LaF_3 NPs. (b) Normalized up-conversion spectra as obtained in presence and absence of 800 nm laser radiation propagating along the waveguide. (c) Laser-induced increment in the surface temperature as a function of the 800 nm laser injected power. Data were obtained at 100 μm from the input face.

In order to get an additional proof of the existence of the intra-waveguide temperature increments of a few degrees, an alternative approach for thermal sensing was carried out. In this case up-converting Erbium:Ytterbium co-doped LaF_3 nanoparticles were deposited on the top of the channel waveguide, as illustrated in Fig. 5(a). Here, the same experimental set-up used for thermal imaging of the waveguide was applied but replacing the "probe" 808-nm by a "probe" 980-nm laser beam. The purpose of this 980 nm beam is to excite, via a two-photon process, the green luminescence of Erbium ions. This technique has been widely used for high sensitivity ratiometric thermal sensing [6]. Basically, temperature sensing was obtained from the analysis of the 500-550 nm emission band of Erbium ions that is constituted by two emission lines generated by two thermally coupled states of erbium ions. A ratiometric analysis of these two emission lines provides an accurate measurement of the nanoparticle´s temperature. Fig. 5(b) shows the two-photon emission spectra generated by the Er:Yb:LaF_3 nanoparticles placed on top of the waveguide at a distance of 100 μm in respect to input face as obtained in either the presence or absence of "pump" 800 nm radiation propagating along the waveguide. It is clear that the presence of the "pump" propagating laser radiation induces a change in the Erbium emission spectrum leading to a increment of the relative contribution of the 545 nm emission line that is unequivocally related to a temperature increment in the Er:Yb:LaF_3 nanoparticles. A quantitative analysis of the emission spectra, based on calibration curves previously reported [21], reveals a laser induced temperature increment close to 7 °C that can be attributed to be the laser-induced temperature increment at the waveguide surface (ΔT_{surf}). The increment in surface temperature was found to increase linearly with the power of injected "pump" 800-nm laser (see Fig. 5(c)), in agreement with the linear trend found in Fig. 4(a). Note that the maximum surface temperature increment is smaller than the maximum temperature increment determined inside the waveguide that is close to 12 °C (Fig. 4(a)). This difference was, indeed, reasonable since temperature is expected to decrease rapidly when moving away from the waveguide core. In any case, results included in Fig. 5 confirm the existence, in our experimental conditions, of laser induced intra-waveguide temperature increments of a few degrees.

In summary, we have demonstrated how luminescence thermometry, in combination with high resolution confocal fluorescence imaging, constitutes a contact-free technique for intra-waveguide thermal imaging. The viability of this technique has been applied to the case of ultrafast laser inscribed Nd:YAG waveguides under real operation conditions. Two main conclusions have been extracted: firstly, for injected laser powers close to 100 mW intra-waveguide laser-induced heating of a few degrees have been experimentally found. Secondly, thermal loading has been demonstrated to be mainly confined at the waveguide´s volume due to the local reduction of thermal conductivity induced at the damage tracks that simultaneous behave as thermal and optical barriers.

Funding. This work was supported by the Spanish Ministerio de Economía y Competitividad (MINECO) under grants MAT2013-47395-C4-1-R and FIS2013-44174-P and from Junta de Castilla y León (Project SA116U13, UIC016).

Acknowledgment. Ruiyun He thanks for the support of China Scholarship Council.

References

1. A. J. Glass, and A. H. Guenther, Appl. Opt. **12,** 637 (1973).
2. M. B. Bavil and E. Safari, J. Mech. Sci. Technol. **28**, 3231 (2014).
3. W. Koechner, Appl. Opt. **9**, 2548 (1970).
4. H. M. Pollock and A. Hammiche, J. Phys. D: Appl. Phys. **34**, R23 (2001).
5. S. Chénais, S. Forget, F. Druon, F. Balembois, and P. Georges, Appl. Phys. B **79**, 221 (2004).
6. C. D. S. Brites, P. P. Lima, N. J. O. Silva, A. Millan, V. S. Amaral, F. Palacio, and L. D. Carlos, Nanoscale **4**, 4799 (2012).
7. D. Jaque and F. Vetrone, Nanoscale **4**, 4301 (2012).
8. J. Petit, B. Viana, and P. Goldner, Opt. Express **19**, 1138 (2011).
9. J. Siebenmorgen, K. Petermann, G. Huber, K. Rademaker, S. Nolte, and A. Tünnermann, Appl. Phys. B **97**, 251 (2009).
10. G. Salamu, F. Jipa, M. Zamfirescu, and N. Pavel, Opt. Mater. Express **4**, 790 (2014).
11. A. G. Okhrimchuk, A. V. Shestakov, I. Khrushchev, and J. Mitchell, Opt. Lett. **30**, 2248 (2005).
12. H. Liu, Y. Jia, J. R. Vázquez de Aldana, D. Jaque, and F. Chen, Opt. Express **20**, 18620 (2012).
13. A. A. Kaminskii, Laser Photonics Rev. **1**, 93 (2007).
14. A. Ródenas, G. A. Torchia, G. Lifante, E. Cantelar, J. Lamela, F. Jaque, L. Roso, and D. Jaque, Appl. Phys. B **95**, 85 (2009).
15. A. Benayas, B. del Rosal, A. Pérez-Delgado, K. Santacruz-Gómez, D. Jaque, G. A. Hirata, and F. Vetrone, Adv. Opt. Mater. **3**, 687 (2015).
16. S. Kobyakov, A. Kamińska, A. Suchocki, D. Galanciak, and M. Malinowski, Appl. Phys. Lett. **88**, 234102 (2006).
17. Y. Bellouard, E. Barthel, A. A. Said, M. Dugan, and P. Bado, Opt. Express **16**, 19520 (2008).
18. A. Benayas, E. Escuder, and D. Jaque, Appl. Phys. B **107**, 697-701 (2012).
19. M. E. Innocenzi, H. T. Yura, C. L. Fincher, and R. A. Fields, Appl. Phys. Lett. **56**, 1831 (1990).
20. A. Benayas, W. F. Silva, C. Jacinto, E. Cantelar, J. Lamela, F. Jaque, J. R. Vázquez de Aldana, G. A. Torchia, L. Roso, A. A. Kaminskii, and D. Jaque, Opt. Lett. **35,** 330-332 (2010).
21. E. C. Ximendes, U. Rocha, C. Jacinto, K. U. Kumar, D. Bravo, F. J. Lopez, E. M. Rodriguez, J. Garcia-Sole, and D. Jaque, Nanoscale **8**, 3057 (2016).

References

1. A. J. Glass, and A. H. Guenther, "Laser Induced Damage of Optical Elements–a Status Report," Appl. Opt. **12,** 637-649 (1973).
2. M. B. Bavil and E. Safari, "Thermal and stress analyses in an end-pumped Nd:YAG slab laser using finite element method," J. Mech. Sci. Technol. **28**, 3231-3236 (2014).
3. W. Koechner, "Thermal lensing in a Nd: YAG laser rod," Appl. Opt. **9**, 2548-2553 (1970).
4. H. M. Pollock and A. Hammiche, "Micro-thermal analysis: techniques and applications," J. Phys. D: Appl. Phys. **34**, R23-R53 (2001).
5. S. Chénais, S. Forget, F. Druon, F. Balembois, and P. Georges, "Direct and absolute temperature mapping and heat transfer measurements in diode-end-pumped Yb : YAG," Appl. Phys. B **79**, 221-224 (2004).
6. C. D. S. Brites, P. P. Lima, N. J. O. Silva, A. Millan, V. S. Amaral, F. Palacio, and L. D. Carlos, "Thermometry at the nanoscale," Nanoscale **4**, 4799-4829 (2012).
7. D. Jaque and F. Vetrone, "Luminescence nanothermometry," Nanoscale **4**, 4301-4326 (2012).
8. J. Petit, B. Viana, and P. Goldner, "Internal temperature measurement of an ytterbium doped material under laser operation," Opt. Express **19**, 1138-1146 (2011).
9. J. Siebenmorgen, K. Petermann, G. Huber, K. Rademaker, S. Nolte, and A. Tünnermann, "Femtosecond laser written stress-induced Nd:$Y_3Al_5O_{12}$ (Nd:YAG) channel waveguide laser," Appl. Phys. B **97**, 251-255 (2009).
10. G. Salamu, F. Jipa, M. Zamfirescu, and N. Pavel, "Cladding waveguides realized in Nd:YAG ceramic by direct femtosecond-laser writing with a helical movement technique," Opt. Mater. Express **4**, 790-797 (2014).
11. A. G. Okhrimchuk, A. V. Shestakov, I. Khrushchev, and J. Mitchell, "Depressed cladding, buried waveguide laser formed in a YAG:Nd^{3+} crystal by femtosecond laser writing," Opt. Lett. **30**, 2248-2250 (2005).
12. H. Liu, Y. Jia, J. R. Vázquez de Aldana, D. Jaque, and F. Chen, "Femtosecond laser inscribed cladding waveguides in Nd:YAG ceramics: Fabrication, fluorescence imaging and laser performance," Opt. Express **20**, 18620-18629 (2012).
13. A. A. Kaminskii, "Laser crystals and ceramics: recent advances," Laser Photonics Rev. **1**, 93-177 (2007).
14. A. Ródenas, G. A. Torchia, G. Lifante, E. Cantelar, J. Lamela, F. Jaque, L. Roso, and D. Jaque, "Refractive index change mechanisms in femtosecond laser written ceramic Nd:YAG waveguides: micro-spectroscopy experiments and beam propagation calculations," Appl. Phys. B **95**, 85-96 (2009).
15. A. Benayas, B. del Rosal, A. Pérez-Delgado, K. Santacruz-Gómez, D. Jaque, G. A. Hirata, and F. Vetrone, "Nd:YAG Near-Infrared Luminescent Nanothermometers, "Adv. Opt. Mater. **3**, 687-694 (2015).
16. S. Kobyakov, A. Kamińska, A. Suchocki, D. Galanciak, and M. Malinowski, "Nd^{3+}-doped yttrium aluminum garnet crystal as a near-infrared pressure sensor for diamond anvil cells," Appl. Phys. Lett. **88**, 234102 (2006).
17. Y. Bellouard, E. Barthel, A. A. Said, M. Dugan, and P. Bado, "Scanning thermal microscopy and Raman analysis of bulk fused silica exposed to low-energy femtosecond laser pulses," Opt. Express **16**, 19520-19534 (2008).
18. A. Benayas, E. Escuder, and D. Jaque, "High-resolution confocal fluorescence thermal imaging of tightly pumped microchip Nd:YAG laser ceramics," Appl. Phys. B **107**, 697-701 (2012).
19. M. E. Innocenzi, H. T. Yura, C. L. Fincher, and R. A. Fields, "Thermal modeling of continuous-wave end-pumped solid-state lasers," Appl. Phys. Lett. **56**, 1831-1833 (1990).
20. A. Benayas, W. F. Silva, C. Jacinto, E. Cantelar, J. Lamela, F. Jaque, J. R. Vázquez de Aldana, G. A. Torchia, L. Roso, A. A. Kaminskii, and D. Jaque, "Thermally resistant waveguides fabricated in Nd:YAG ceramics by crossing femtosecond damage filaments," Opt. Lett. **35,** 330-332 (2010).
21. E. C. Ximendes, U. Rocha, C. Jacinto, K. U. Kumar, D. Bravo, F. J. Lopez, E. M. Rodriguez, J. Garcia-Sole, and D. Jaque, "Self-monitored photothermal nanoparticles based on core-shell engineering," Nanoscale **8**, 3057-3066 (2016).